

Universality in the three-dimensional random bond quantum Heisenberg antiferromagnet

U. Kanbur

*The Graduate School of Natural and Applied Sciences,
Dokuz Eylül University, 35160 Izmir, Turkey and
Department of Physics, Karabük University, Demir Çelik Campus, 78050 Karabük, Turkey*

E. Vatansever* and H. Polat

*Department of Physics, Dokuz Eylül University, TR-35160 Izmir, Turkey
(Dated: August 5, 2020)*

The three-dimensional quenched random bond diluted ($J_1 - J_2$) quantum Heisenberg antiferromagnet is studied on a simple-cubic lattice. Using extensive stochastic series expansion quantum Monte Carlo simulations, we perform very long runs for $L \times L \times L$ lattice up to $L = 48$. By employing standard finite-size scaling method, the numerical values of the Néel temperature are determined with high precision as a function of the coupling ratio $r = J_2/J_1$. Based on the estimated critical exponents, we find that the critical behavior of the considered model belongs to the pure classical 3D $O(3)$ Heisenberg universality class.

I. INTRODUCTION

The concept of disorder and randomness on the critical and universality properties of the magnetic materials have great importance for the understanding of the statistical and condensed matter physics¹⁻¹⁶. However, clarifying the influence of the disorder and randomness effects on the critical exponents of second-order phase transitions has so far been a challenge. It has been demonstrated that there are several approaches to introducing randomness in magnetic materials¹⁷, e.g. the presence of random exchange couplings between interacting spins, or the dilution of magnetic ions. It is a known fact that most of the magnetic materials are more or less defective. Therefore, zero- and finite-temperature physical properties of the samples can significantly change depending on the kind and amount of defects. They often show unusual and interesting magnetic behaviors that are prominently different from that of their pure counterparts^{9,12,13,15}. As an example, it has been given in Ref.⁹ that all critical exponents including dynamical correlations are different from the classical percolation values, leading to a novel universality class for the percolation quantum phase transition in quantum magnets with quenched disorder.

Among the many spin models, one of the most studied is the Heisenberg model, both from numerical and analytical points of view. It builds a strong bridge between the experiments and computer simulations in condensed matter physics. In this context, it allows us to explore the underlying physics of the pure and disordered magnetic materials where the spin-spin correlations are important. Until the present day, ground state, finite-temperature, and also universality properties of the many one-dimensional (1D) and two-dimensional (2D) magnetic systems including different kinds of disorders have been comprehensively investigated through a variety of numerical and theoretical methods. Examples include quantum spin models

with random bonds^{2,3,18-24}, site dilution^{4,5,25-32}, isolated impurity³³, frustration effects³⁴⁻⁴⁰, $J - Q$ terms^{16,41-44} and dimerized $J_1 - J_2$ systems⁴⁵⁻⁵¹. Magnetic properties of the $S = 1/2$ Heisenberg antiferromagnet on an inhomogeneous 2D square lattice have been studied by employing quantum Monte Carlo (QMC) simulation in Ref.⁴⁵. The critical exponent ν of the correlation length is estimated using finite-size scaling (FSS) analysis, which is consistent with the three-dimensional $O(3)$ classical Heisenberg universality class ($\nu \approx 0.71$)^{52,53}. The same confirmation of the $O(3)$ universality class has also been shown by Wenzel and Janke in Ref.⁴⁷ for the two planar square lattice Heisenberg models with explicit dimerization or quadrumerization, by making use of the stochastic series expansion (SSE) QMC technique. The detailed works in the existing literature prove that our understanding of critical phenomena of the disordered and clean 1D and 2D quantum magnets has reached a point where well-established results are available, as mentioned above. There are, however, quite limited studies on the universality properties of the disordered three-dimensional (3D) quantum spin systems. This may be due to the limitation in the computational resources that require the averaging of physical observables over a large number of experiments.

To the best of our knowledge, most of the studies - inspired by the experimental observation of TiCuCl_3 under pressure⁶²⁻⁶⁴ - have been recently performed on different kinds of 3D quantum antiferromagnetic pure and disordered dimerized lattices and have focused on the estimation of the scaling relations of Néel temperature (T_N) and the staggered magnetization density (M_s) near a quantum critical point⁵⁴⁻⁶¹. Related to this, the first theoretical attempts have been carried out using quantum field theory, and the existence of universal behavior near the quantum critical point has been demonstrated^{54,55}. In turn, using QMC simulations, Jin and Sandvik have proposed a way to relate T_N to M_s of the ground state for the several kinds of pure dimerized systems. Ana-

lyzing the numerical data, they have found an almost perfect universality⁵⁶. In Ref.⁵⁸, universal scaling of T_N and M_s of the 3D random-exchange quantum antiferromagnets have been investigated within the framework of QMC simulations. The authors have reported that the obtained numerical results support the scaling relations observed for the pure systems for the model including quenched disorder. A similar confirmation of the universal scaling relations of the relevant physical quantities has been also found for the 3D quantum antiferromagnet with configurational disorder⁵⁹. These studies indicate that the scaling properties of the 3D quantum antiferromagnets are universal in the quantum critical regime, and valid for both pure and disordered models. Since T_N and M_s are physical observables, the data collapse of these terms has a great significance for experimental physics. Hence, it is evident that most of the attention has been dedicated to clarifying the scaling relations between T_N and M_s . There are, however, still unresolved issues regarding the behavior of the 3D quantum Heisenberg model in the existence of quenched disorder. Some of the questions waiting for an answer are given as follows: (i) What is the effect of the disorder on the critical temperature of the system? (ii) What will be the universality class of the resulting phase transitions? In other words, do the obtained critical exponents depend on the amount of disorder? In this paper, we consider the 3D random-bond quantum antiferromagnetic Heisenberg model with a different perspective. More specifically, our motivation is to obtain an answer for the above questions, and in this way, to determine the universality properties of the 3D quantum Heisenberg model in the presence of quenched disorder, employing extensive SSE QMC simulations. In a nutshell, our numerical findings indicate that phase transitions of the 3D quantum Heisenberg antiferromagnet with quenched disorder belong to the $O(3)$ universality class of the pure 3D classical Heisenberg model^{52,53}.

The outline of the paper is as follows: In Sec. II, we give the model and the details of the simulation scheme. The numerical results and discussion are discussed in Sec. III, and finally, Sec. IV contains a summary of our conclusions.

II. MODEL AND SIMULATION DETAILS

It is more convenient and compact to express the Hamiltonian of the model in terms of the bond interactions and putting restrictions on the created bonds to represent the system of interest. Namely, the Hamiltonian,

$$\mathcal{H} = \sum_{b=1}^{N_b} J_b \mathbf{S}_{i(b)} \cdot \mathbf{S}_{j(b)} \quad (1)$$

describes the spin models that include N_b number of bonds with site index $i(b)$ and spin operators $\mathbf{S}_{i(b)}$ inter-

acting with coupling strength J_b . For this model, all the interactions are antiferromagnetic ($J_b > 0$) and among the nearest-neighbor sites on a cubic lattice. These bonds are randomly selected from a bimodal distribution, which is given as follows:

$$\mathcal{P}(J_b) = \frac{1}{2} [\delta(J_b - J_1) + \delta(J_b - J_2)]. \quad (2)$$

Following Refs.⁶⁵⁻⁶⁸ we chose $J_1 + J_2 = 2$ and $J_1 > J_2 > 0$; so $r = J_2/J_1$ defines the disorder strength. It is clear that $r = 1$ corresponds to the pure 3D spin-1/2 Heisenberg AFM. Among the previously published studies regarding the critical properties of the pure model, QMC simulations suggest the location of the transition temperature between Néel and paramagnetic phases as $k_B T_N/J = 0.946(1)$ ⁶⁹ and 0.947 ⁷⁰.

Within the framework of the SSE technique for the isotropic $S = 1/2$ Heisenberg antiferromagnetic model, the bond operators are split into diagonal and off-diagonal terms as follows,

$$H_{1,b} = \left(\frac{1}{4} - S_{i(b)}^z S_{j(b)}^z \right) \quad (3a)$$

$$H_{2,b} = \frac{1}{2} \left(S_{i(b)}^+ S_{j(b)}^- + S_{i(b)}^- S_{j(b)}^+ \right) \quad (3b)$$

where $H_{1,b}$ and $H_{2,b}$ are diagonal and off-diagonal bond operators, respectively. Then we write the Hamiltonian over the bond operators by indicating random coupling strengths explicitly,

$$\mathcal{H} = - \sum_{b=1}^{N_b} J_b (H_{1,b} - H_{2,b}) + \text{const.} \quad (4)$$

The constant term in Eq. (4) does not affect the computed quantities except for the internal energy and can be included in the post-simulation calculations if desired. According to the SSE technique^{71,74,75}, the partition function is expanded to the Taylor series with a chosen basis,

$$\mathcal{Z} = \sum_{\alpha, S_L} (-1)^{n_2} \beta^n \frac{(L-n)!}{L!} \left\langle \alpha \left| \prod_{p=0}^{L-1} J_{b(p)} H_{a(p), b(p)} \right| \alpha \right\rangle, \quad (5)$$

which is a sum over configurations α and all possible operator strings S_L including a unit operator $H_{0,0}$ to make the length of the strings fixed and a unit bond coupling for a convenient implementation and for this extra index we have $J_0 \equiv 1$. In this scheme, n turns out to be the number of non-unit operators in the string, and n_2 is the number of off-diagonal operators that appear in pairs in the operator string for a bipartite system thus making the matrix elements always positive and β is a reduced inverse temperature with Boltzmann constant. All the non-zero matrix elements are $J_b/2$ and the weight

is given as follows,

$$W(\alpha, S_L) = \left(\frac{\beta}{2}\right)^n \frac{(L-n)!}{L!} \prod_{p=0}^{L-1} J_{b(p)}. \quad (6)$$

The relevant quantities are measured for the analysis of thermal and critical behavior by making simulations at different system sizes and temperatures for each disorder parameter. In our simulations, $N = L \times L \times L$ defines the total number of spins while L denotes the linear dimension of the lattice, having the values $L = 4, 6, 8, 12, 16, 24, 32$ and 48 . We apply the boundary conditions such that they are periodic in all directions. The simulations have been realized for three coupling ratios, namely $r = 0.9/1.1, 0.75/1.25$ and $0.5/1.5$. For each pair of (L, r) , we performed 300 independent experiments, generating random seeds. In each sample realizations, the first 10^5 Monte Carlo steps (MCS)⁷¹ are discarded for thermalization process, and the numerical data are collected over the next 5×10^5 MCS. After determining the critical temperature region for each disorder parameter, the running averages of the specific heat values at a temperature very close to the critical point are monitored to ensure the sufficiency of the number of independent realizations. As an example, it is clear from Fig. 1 that 300 random realizations are found to be enough for the statistics of the calculations for the disordered model with parameter $r = 0.75/1.25$. We also note that the simulations are performed on a cluster with processors Intel(R) Xeon(R) Gold 6148 CPU @ 2.40GHz and actual running times in the critical region are measured up to approximately ten days for $L = 48$ and a single random realization.

Similar averages are also observed for other disorder parameters, which are not shown here. The formulation of SSE QMC allows one to derive simple estimators for the quantities of interest. The specific heat estimator (C) is defined by the number of non-unit operators⁷⁴,

$$C = \langle n^2 \rangle - \langle n \rangle^2 - \langle n \rangle. \quad (7)$$

In the SSE formalism, the Kubo integral can be discretized in a compact form including all the propagated states in the imaginary time⁷⁵, that reduces to staggered susceptibility (χ_s), which can be defined as follows:

$$\chi_s(\mathbf{Q}) = \left\langle \frac{\beta}{n(n+1)} \left[\left(\sum_{k=0}^{n-1} M_s^z(k) \right)^2 + \sum_{k=0}^{n-1} (M_s^z(k))^2 \right] \right\rangle, \quad (8)$$

where $\mathbf{Q} = (\pi, \pi, \pi)$ is the 3D ordering wave vector while M_s^z is the staggered magnetization, which is given below,

$$M_s^z = \frac{1}{N} \sum_{i=1}^N S_i^z (-1)^{x_i+y_i+z_i}. \quad (9)$$

The dimensionless Binder parameters are defined as fol-

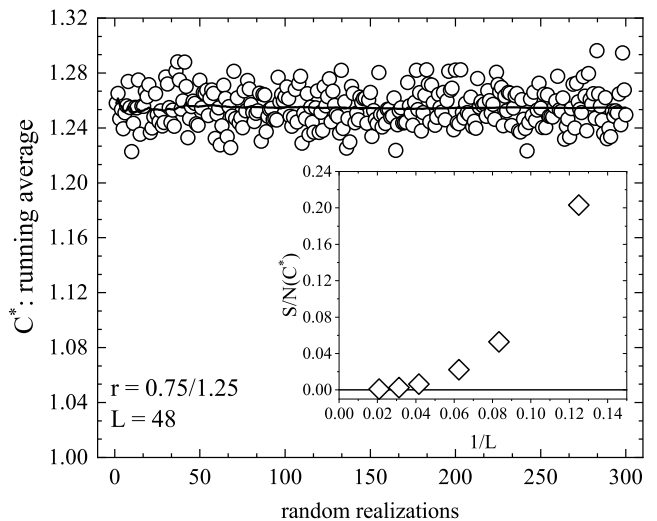


FIG. 1. (Color online) Disorder distributions of the specific heat maxima (C^*) for a lattice size $L = 48$ for the model with $r = 0.75/1.25$. The running averages over the samples are illustrated by a solid line. Inset shows the signal-to-noise S/N ratio of the specific heat as a function of the inverse system size. $S/N(C^*) \rightarrow 0$ when $1/L \rightarrow 0$, indicating that self-averaging is restored in the thermodynamic limit for the 3D bond-diluted quantum Heisenberg AFM model^{72,73}.

lows:

$$Q_2 = \frac{\langle (M_s^z)^2 \rangle}{\langle |M_s^z|^2 \rangle}, \quad (10)$$

$$Q_4 = \frac{\langle (M_s^z)^4 \rangle}{\langle (M_s^z)^2 \rangle^2}, \quad (11)$$

and they are independent of the system size at T_N . Another quantity is the spin stiffness that has a scaling behavior at the critical point defined as the response to a boundary twist (ϕ) and is given as (for quantum systems)

$$\rho = \frac{1}{N} \left. \frac{\partial^2 E(\phi)}{\partial \phi^2} \right|_{\phi \rightarrow 0}, \quad (12)$$

where $E(\phi)$ is the energy of the twisted Hamiltonian. The estimator for spin stiffness can be deduced from the Kubo integral by averaging a non-diagonal spin current operator^{71,76}, which gives a result in terms of the winding number. For the present model (isotropic) we can improve the value of ρ by averaging the estimator for each dimension,

$$\rho = \frac{1}{3\beta} \sum_{\alpha} \langle W_{\alpha}^2 \rangle, \quad \alpha \in \{x, y, z\} \quad (13)$$

where

$$\omega_{\alpha} = \frac{1}{L} (N_{\alpha}^+ - N_{\alpha}^-), \quad (14)$$

is the winding number in α direction. The numbers N_α^+ and N_α^- count the operators $S_{i(b)}^+ S_{j(b)}^-$ and $S_{i(b)}^- S_{j(b)}^+$, respectively, on bond b in the relevant direction. The essence of the SSE technique, implemented for the present and similar systems, is based on the operator loops^{71,74} that can take into account winding number sectors exactly thus making the spin stiffness a reliable quantity for critical analysis.

III. RESULTS AND DISCUSSION

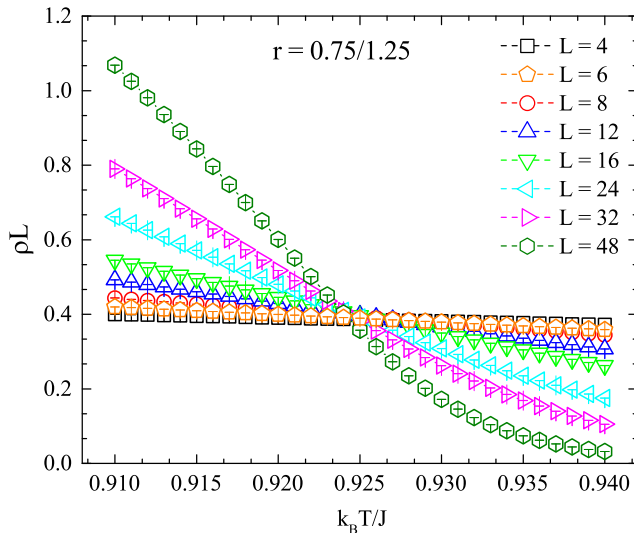


FIG. 2. (Color online) Thermal variation of ρL for varying values of system sizes: $L = 4, 6, 8, 12, 16, 24, 32$ and 48 . All curves are obtained for $r = 0.75/1.25$. The dashed lines are added to guide the eye.

There are several ways to determine the Néel temperature $k_B T_N/J$ of the considered system. We use three physical quantities: the spin stiffness (ρ), and the dimensionless Binder ratios Q_2 and Q_4 , for all selected coupling ratios r . We first consider the system size and temperature dependence of ρ . It should be noted here that ρ can be measured from the global winding number fluctuations in the system, within the framework of SSE QMC⁷⁷. According to the hyperscaling theory, finite-size scaling of the spin stiffness can be written as $\rho = L^{2-d-z}$ at the phase transition point⁷⁸. Here d is the dimension of the system (as noted before, $d = 3$ in our study) while z is the dynamic critical exponent which is zero for finite-temperature phase transitions. Therefore, $L\rho$ is independent of L at $k_B T_N/J$, which means that the curves versus reduced temperature displays an intersection point for two selected different system sizes. We give thermal variations of ρL for $L = 4, 6, 8, 12, 16, 24, 32$ and 48 at fixed coupling ratio $r = 0.75/1.25$, as depicted in Fig. 2. It is clear from the figure that ρL tends to vanish for $k_B T/J > k_B T_N/J$ whereas it begins to increase

in the range of $k_B T/J < k_B T_N/J$. The curves corresponding to the different pairs of L as a function of the temperature intersects almost a single point showing a sign of a phase transition between antiferromagnetic and paramagnetic phases.

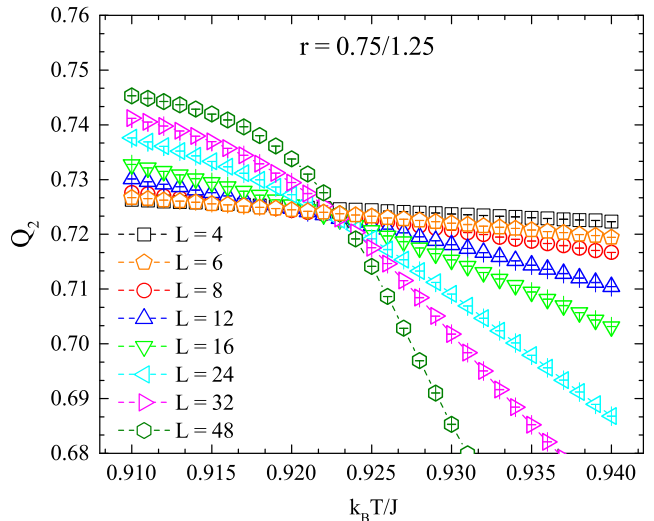


FIG. 3. (Color online) Thermal variation of Q_2 for varying values of system sizes: $L = 4, 6, 8, 12, 16, 24, 32$ and 48 . All curves are obtained for $r = 0.75/1.25$. The dashed lines are added to guide the eye.

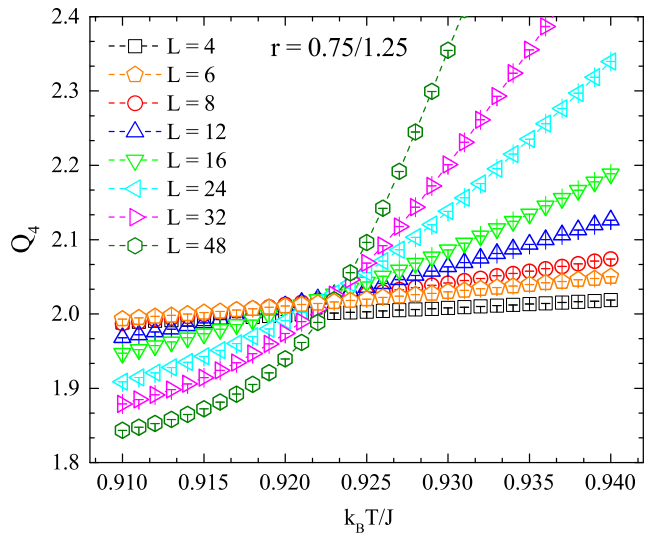


FIG. 4. (Color online) Thermal variation of Q_4 for varying values of system sizes: $L = 4, 6, 8, 12, 16, 24, 32$ and 48 . All curves are obtained for $r = 0.75/1.25$. The dashed lines are added to guide the eye.

In Figs. 3 and 4, thermal variations of Q_2 and Q_4 are depicted for the system with the size $L = 4, 6, 8, 12, 16, 24, 32$ and 48 at fixed coupling ratio $r = 0.75/1.25$. In these figures, we observe that the curves corresponding to varying system sizes tend to cross with

each other in the vicinity of phase transition of the system.

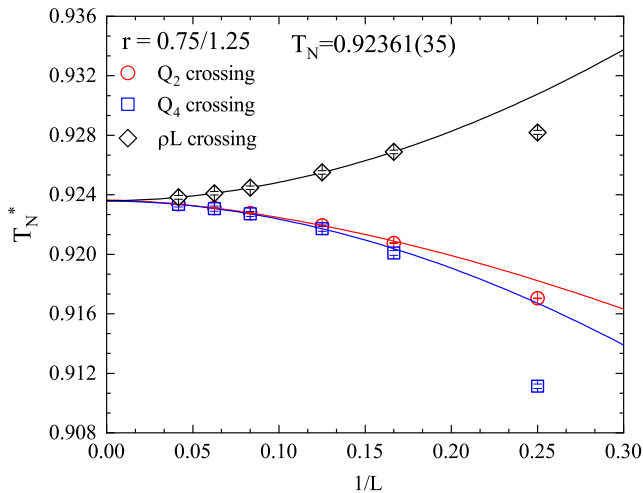


FIG. 5. (Color online) Crossing points of the pair of the system sizes $(L, 2L)$ for ρL , Q_2 and Q_4 as a function of $1/L$. Lines are fits to the equation: $T_N^*(L) = T(\infty) + aL^{-\omega}$. All curves are obtained for $r = 0.75/1.25$.

We use the numerical data given for ρL , Q_2 and Q_4 to obtain the intersection point of fixed L curves for the pairs of $(L, 2L)$. It is worth noting that the numerical data have been collected using a very small temperature step $\Delta k_B T/J = 10^{-3}$ for the chosen temperature regions. Therefore, we can obtain the intersection point with high accuracy using the reliable power-law fits to extrapolate to infinite size, i.e., $L \rightarrow \infty$ limit. We give $1/L$ dependence of T_N^* , where the relevant quantities cross with each other, as displayed in Fig. 5. In this figure, the solid lines are fits to the function $T_N^*(L) = T_\infty + aL^{-\omega}$. Here, a is a constant, and ω is the crossing point shift exponent⁷¹. When the relevant data points with $L \geq 8$, the scaling function begins to behave well. All the extrapolated values indicate that the Néel temperature is 0.92361(35) for the fixed coupling ratio $r = 0.75/1.25$. Remarkably, it is clear from the figure that spin stiffness crossing points converge this value from above while the dimensionless Binder ratios converge from below. We note that similar types of observation mentioned here have been also found in a variety of quantum spin models. Two notable examples are the $S = 1/2$ Quantum Heisenberg bilayers⁷⁹ and dimerized/quadrumerized Heisenberg models⁴⁷, where the corresponding quantum phase transition points have been extracted in detail, instead of thermal phase transition observed here. We obtain the critical temperatures for the remaining selected coupling ratios, using the same procedure followed for $r = 0.75/1.25$. Our Monte Carlo simulations suggest that the critical temperatures are 0.94075(3) and 0.861613(12) for $r = 0.9/1.1$ and $r = 0.5/1.5$, respectively. These results will be used to estimate the critical exponents and check the data collapse treatment of the staggered sus-

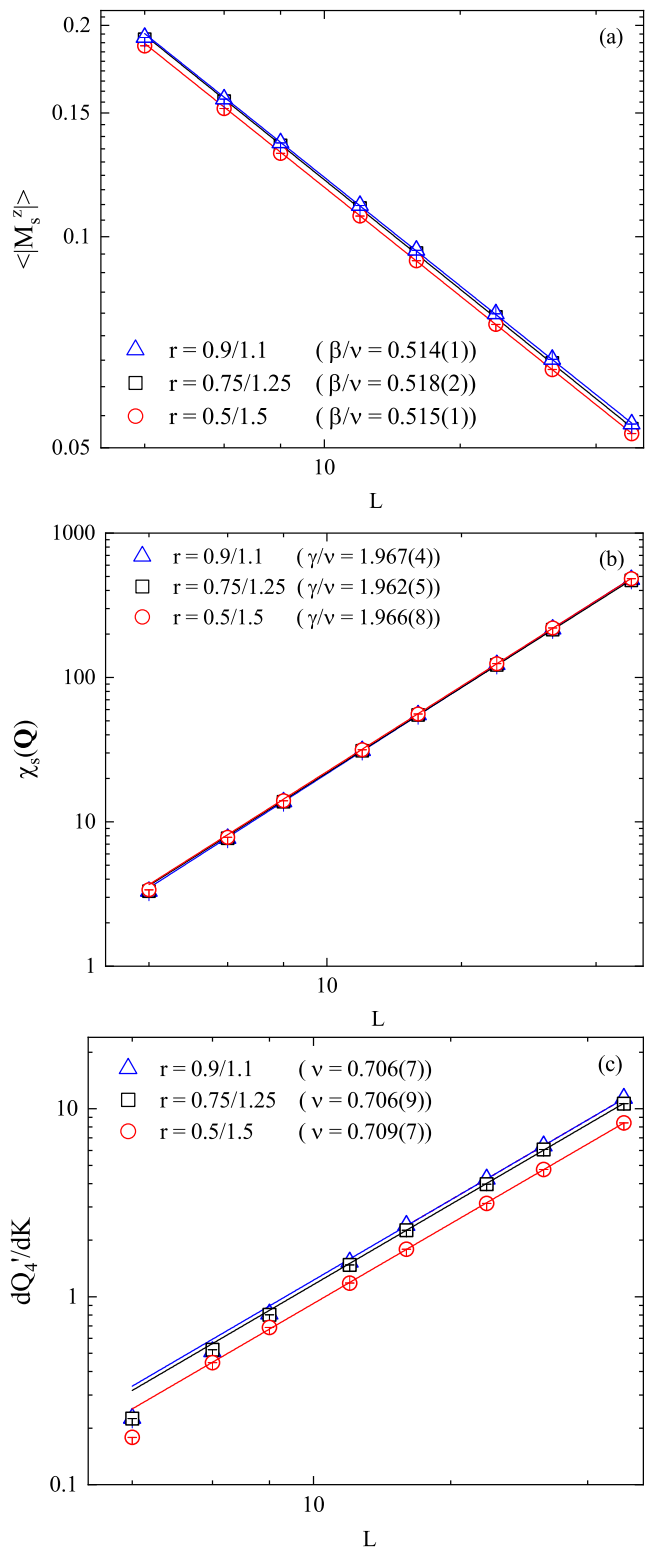


FIG. 6. (Color online) Log-log plots of the magnetization $\langle |M_s^z| \rangle$ (a), staggered susceptibility $\chi_s(Q)$ (b) and derivative of the Binder cumulant dQ_4/dK (c) versus the system with the sizes $L = 4, 6, 8, 12, 16, 24, 32$ and 48 . All curves are obtained for the considered coupling ratios of $r = 0.9/1.1$, $r = 0.75/1.25$ and $r = 0.5/1.5$.

ceptibility and scaling behaviors of the system.

Having determined critical temperatures, we proceed now with testing the expected scaling behavior of the system for all considered coupling ratios r . According to the standard FSS theory of the equilibrium magnetization $\langle |M_s^z| \rangle$ at the critical point, the following power-law can be used to obtain β/ν exponent:

$$\langle |M_s^z| \rangle \sim L^{-\beta/\nu}, \quad (15)$$

where β is the critical exponent of the magnetization. Figure 6(a) shows the log-log plots of the staggered magnetization versus the system with varying sizes L . Power-law fits of the form of Eq. (15) give the critical exponent ratios as $\beta/\nu = 0.514(1), 0.518(2)$ and $0.515(1)$ for the coupling ratios $r = 0.9/1.1, 0.75/1.25$ and $0.5/1.5$, respectively. In addition to β/ν , we find the critical exponent ratio γ/ν of the staggered susceptibility curve, which can be estimated by benefiting from the following power-law^{80,81}:

$$\chi_s(\mathbf{Q}) \sim L^{\gamma/\nu}. \quad (16)$$

here γ denotes the critical exponent of the staggered susceptibility. From the log-log plot, our numerical findings suggest that the values of the exponent ratios are $\gamma/\nu = 1.967(4), 1.962(5)$ and $1.966(8)$ corresponding to the chosen coupling ratios $r = 0.9/1.1, 0.75/1.25$ and $0.5/1.5$, respectively, as depicted in Figure 6(b). Further evidence can be provided via the critical exponent ν of the correlation length. A simple way to estimate ν is to use the derivative of the Binder cumulant at the critical point. It should obey the relation⁸²:

$$\frac{dQ'_4}{dK} \sim L^{1/\nu}, \quad (17)$$

where $Q'_4 = 1 - Q_4/3$ and K is the inverse temperature, i.e., $K = 1/k_B T$. Power-law fits of the form Eq. (17) are displayed in Figure 6(c). Our simulation results indicate that the critical exponents for the correlation lengths are estimated as $\nu = 0.706(7), 0.706(9)$ and $0.709(7)$ for the studied coupling ratios $r = 0.9/1.1, 0.75/1.25$ and $0.5/1.5$, respectively. To briefly summarize, in the view of the critical exponents estimated above (i.e., $\beta/\nu, \gamma/\nu$ and ν), it is possible to say that the critical exponents are in excellent agreement with the classical 3D $O(3)$ Heisenberg model exponents^{52,53}.

For a final verification of the 3D $O(3)$ Heisenberg universality class, we now continue with testing the expected scaling behavior of the system for $T \geq T_N$ for all considered coupling ratios r . In the thermodynamic limit, the susceptibility diverges as $\chi \sim |t|^{-\gamma}$, where $t = T - T_N$. Finite-size scaling theory also predicts $\chi_L(t) = \chi_\infty(t)f[\xi(t)/L]$. Here, ξ ($\sim t^{-\nu}$) is the correlation length^{80,81}. Based on this definition, it is possible to say that $\chi_L(t)t^\gamma$ versus Lt^ν curves corresponding to the varying system sizes should collapse onto a single curve. We give the FSS scaling behavior of the staggered susceptibilities in the vicinity of phase transition points

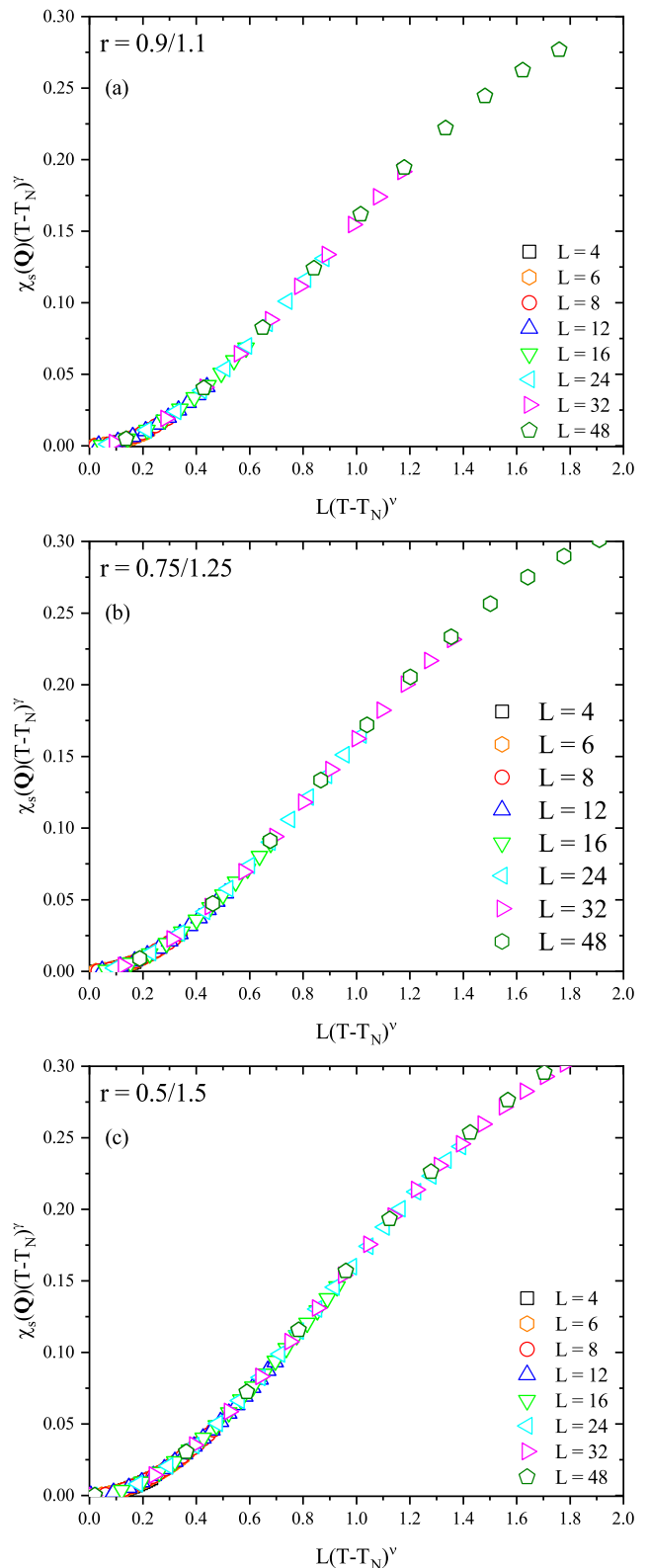


FIG. 7. (Color online) Finite-size scaling of the staggered susceptibility above the Néel temperature for the systems with $L = 4, 6, 8, 12, 16, 24, 32$ and 48 . All curves are obtained for the considered coupling ratios of (a) $r = 0.9/1.1$, (b) $r = 0.75/1.25$ and (c) $r = 0.5/1.5$. The error bars are smaller than the symbols.

of the system with the sizes $L = 4, 6, 8, 12, 16, 24, 32$ and 48 in Fig. 7. Specifically, we display the curves referring to the varying values of coupling ratios $r = 0.9/1.1, 0.75/1.25$ and $0.5/1.5$, in Figs. 7(a), (b) and (c) respectively. For this, γ and ν exponent pairs have been used for each coupling ratio r . Remarkably, the data collapse behavior observed here provides a strong indication of the $3D$ $O(3)$ Heisenberg universality in the second-order regime of the $3D$ antiferromagnetic quantum Heisenberg model in the presence of quenched disorder.

IV. CONCLUSION

In the present paper we have investigated the effects of quenched disorder on the critical and universality properties of the $3D$ quantum Heisenberg antiferromagnetic model. Specifically, we have realized large-scale SSE-QMC simulations on a simple cubic lattice with the system size L up to $L = 48$ at various values of coupling ratios r . First, we have obtained the crossing point of $\rho L, Q_2$ and Q_4 , then present the FSS behavior of the considered model to estimate the critical temperatures with high accuracy for all selected coupling ratios r . Having determined critical temperatures, we have studied the universality class of the disordered model, based on the critical exponents and data collapse analysis. Our simulation results indicate that the critical behavior observed for the considered model belong to the universality class of the pure classical $3D$ $O(3)$ Heisenberg universality class^{52,53}. The results given in this study also strongly

support the fact that the universality properties of the system do not depend on the microscopic details of the Hamiltonian, i.e., spin-spin interactions.

An important concept concerning the disordered systems is the Harris criterion which states that the critical behavior of a pure system is stable against a disorder if the condition $d\nu \geq 2$ is satisfied. If the inequality does not meet for the pure case of the model, a new universality class with a new correlation length exponent ν satisfying the criterion is expected to emerge⁸³. The condition $d\nu > 2$ holds for the clean case of the present model. Based on the outcomes reported in this paper, we conclude that the Harris criterion is not violated since the critical exponents found not to change upon the presence of random bond couplings. Hence, the Harris criterion provides insight into the criticality of the $3D$ Heisenberg model with bimodal quenched disorder.

Finally, it would be interesting to investigate a new, alternative approach for the stacked honeycomb lattices in $3D$ geometry. A new model considering random bond dilution could provide a further understanding of the critical behaviors observed in the disordered magnetic systems.

ACKNOWLEDGEMENTS

The authors would like to thank S. Wessel, F.-J. Jiang and D.-X. Yao for many useful comments and discussion on the manuscript. The numerical calculations reported in this paper were performed at TÜBİTAK ULAKBİM, High Performance and Grid Computing Center (TR-Grid e-Infrastructure).

* erol.vatansever@deu.edu.tr

¹ Spin Glasses and Random Fields, edited by A. P. Young (World Scientific, Singapore, 1997).

² A.W. Sandvik, Phys. Rev. B **50**, 15803 (1994).

³ A.W. Sandvik and M. Vekić, Phys. Rev. Lett. **74**, 1226 (1995).

⁴ S. Wessel, B. Normand, M. Sgrist, and S. Haas, Phys. Rev. Lett. **86**, 1086 (2001).

⁵ A.L. Chernyshev, Y.C. Chen, and A.H. Castro Neto, Phys. Rev. Lett. **87**, 067209 (2001)

⁶ A.W. Sandvik, Phys. Rev. Lett. **89**, 177201 (2002).

⁷ K.H. Höglund and A.W. Sandvik, Phys. Rev. Lett. **91**, 077204 (2003).

⁸ S. Sachdev and M. Vojta, Phys. Rev. B **68**, 064419 (2003).

⁹ T. Vojta and J. Schmalian, Phys. Rev. Lett. **95**, 237206 (2005).

¹⁰ N. Laflorencie, S. Wessel, A. Läuchli, and H. Rieger, Phys. Rev. B **73**, 060403(R) (2006).

¹¹ Y.-C. Lin, H. Rieger, N. Laflorencie, and F. Iglói, Phys. Rev. B **74**, 024427 (2006).

¹² T. Vojta and M. Y. Lee, Phys. Rev. Lett. **96**, 035701 (2006).

¹³ A.W. Sandvik, Phys. Rev. Lett. **96**, 207201 (2006).

¹⁴ K.H. Höglund and A.W. Sandvik, Phys. Rev. Lett. **99**, 027205 (2007).

¹⁵ A.K. Ibrahim and T. Vojta, Phys. Rev. B **95**, 054403 (2017).

¹⁶ L. Liu, H. Shao, Y.-C. Lin, W. Guo, and A.W. Sandvik, Phys. Rev. X **8**, 041040 (2018).

¹⁷ T. Vojta, Annu. Rev. Condens. Matter Phys. **10**, 233 (2019).

¹⁸ D.S. Fisher, Phys. Rev. B **50**, 3799 (1994).

¹⁹ B. Frischmuth and M. Sgrist, Phys. Rev. Lett. **79**, 147 (1997).

²⁰ S. Bergkvist, P. Henelius, and A. Rosengren, Phys. Rev. B **66**, 134407 (2002).

²¹ K. Hamacher, J. Stolze, and W. Wenzel, Phys. Rev. Lett. **89**, 127202 (2002).

²² C. Yasuda, S. Todo, M. Matsumoto, and H. Takayama, J. Phys. Chem. Solids **63**, 1607 (2002).

²³ T. Fabritius, N. Laflorencie, and S. Wessel, Phys. Rev. B **82**, 035402 (2010).

²⁴ T. Shimokawa, K. Watanabe, and H. Kawamura, Phys. Rev. B **92**, 134407 (2015).

²⁵ C.C. Wan, A.B. Harris, and J. Adler, J. Appl. Phys. **69**, 5191 (1991).

²⁶ J. Behre and S. Miyashita, J. Phys. A: Math. Gen. **25**, 4745 (1992).

²⁷ K. Kato, S. Todo, K. Harada, N. Kawashima, S. Miyashita, and H. Takayama, Phys. Rev. Lett. **84**, 4204 (2000).

- ²⁸ A.W. Sandvik, Phys. Rev. Lett. **86**, 3209 (2001).
- ²⁹ C. Yasuda, S. Todo, M. Matsumoto, and H. Takayama, Phys. Rev. B **64**, 092495 (2001).
- ³⁰ A.L. Chernyshev, Y.C. Chen, and A.H. Castro Neto, Phys. Rev. B **65**, 104407 (2002).
- ³¹ O.P. Vajk and M. Greven, Phys. Rev. Lett. **89**, 177202 (2002).
- ³² R. Yu, O. Nohadani, S. Haas, and T. Roscilde, Phys. Rev. B **82**, 134437 (2010).
- ³³ S. Eggert and I. Affleck, Phys. Rev. B **46**, 10866 (1992).
- ³⁴ A.F. Albuquerque, D. Schwandt, B. Hetényi, S. Capponi, M. Mambrini, and A.M. Läuchli, Phys. Rev. B **84**, 024406 (2011).
- ³⁵ R.F. Bishop, P.H.Y. Li, D.J.J. Farnell, J. Richter, and C.E. Campbell, Phys. Rev. B **85**, 205122 (2012).
- ³⁶ S Furukawa, M. Sato, S. Onoda, and A. Furusaki, Phys. Rev. B **86**, 094417 (2012).
- ³⁷ R.F. Bishop, P.H.Y. Li, O. Götze, J. Richter, and C.E. Campbell, Phys. Rev. B **92**, 224434 (2015).
- ³⁸ S.-S. Gong, W. Zhu, and D.N. Sheng, Phys. Rev. B **92**, 195110 (2015).
- ³⁹ F. Alet, K. Damle, and S. Pujari, Phys. Rev. Lett. **117**, 197203 (2016).
- ⁴⁰ J. Stapmanns, P. Corboz, F. Mila, A. Honecker, B. Normand, and S. Wessel, Phys. Rev. Lett. **121**, 127201 (2018).
- ⁴¹ A.W. Sandvik, Phys. Rev. Lett. **104**, 177201 (2010).
- ⁴² A. Iaizzi, K. Damle, and A.W. Sandvik, Phys. Rev. B **95**, 174436 (2017).
- ⁴³ A. Iaizzi, K. Damle, and A.W. Sandvik, Phys. Rev. B **98**, 064405 (2018).
- ⁴⁴ B. Zhao, P. Weinberg, A.W. Sandvik, Nat. Phys. **15**, 678 (2019).
- ⁴⁵ A.F. Albuquerque, M. Troyer, and J. Oitmaa, Phys. Rev. B **78**, 132402 (2008).
- ⁴⁶ S. Wenzel, L. Bogacz, and W. Janke, Phys. Rev. Lett. **101**, 127202 (2008).
- ⁴⁷ S. Wenzel and W. Janke, Phys. Rev. B **79**, 014410 (2009).
- ⁴⁸ D.-X. Yao, J. Gustafsson, E.W. Carlson, and A.W. Sandvik, Phys. Rev. B **82**, 172409 (2010).
- ⁴⁹ L. Fritz, R.L. Doretto, S. Wessel, S. Wenzel, S. Burdin, and M. Vojta, Phys. Rev. B **83**, 174416 (2011).
- ⁵⁰ F.-J. Jiang, Phys. Rev. B **85**, 014414 (2012).
- ⁵¹ X. Ran, N. Ma, and D.-X. Yao, Phys. Rev. B **99**, 174434 (2019).
- ⁵² P. Peczak, A.M. Ferrenberg, and D.P. Landau, Phys. Rev. B **43**, 6087 (1991).
- ⁵³ M. Campostrini, M. Hasenbusch, A. Pelissetto, P. Rossi, and E. Vicari, Phys. Rev. B **65**, 144520 (2002).
- ⁵⁴ Y. Kulik, O.P. Sushkov, Phys. Rev. B **84**, 134418 (2011).
- ⁵⁵ J. Oitmaa, Y. Kulik, O.P. Sushkov, Phys. Rev. B **85**, 134431 (2012).
- ⁵⁶ S. Jin and A.W. Sandvik, Phys. Rev. B **85**, 020409(R) (2012).
- ⁵⁷ M.T. Kao and F.-J. Jiang, Eur. Phys. B **86**, 413 (2013).
- ⁵⁸ D.-R. Tan and F.-J. Jiang, Eur. Phys. B **88**, 289 (2015).
- ⁵⁹ D.-R. Tan and F.-J. Jiang, Phys. Rev. B **95**, 054435 (2017).
- ⁶⁰ D.-R. Tan, C.-D. Li, and F.-J. Jiang, Phys. Rev. B **97**, 094405 (2018).
- ⁶¹ D.-R. Tan, and F.-J. Jiang, Phys. Rev. B **101**, 054420 (2020).
- ⁶² Ch. Rüegg, N. Cavadini, A. Furrer, H.-U. Güdel, K.W. Krämer, H. Mutka, A. Wildes, K. Habicht, and P. Vorderwisch, Nature, **423** 62 (2003).
- ⁶³ Ch. Rüegg, B. Normand, M. Matsumoto, A. Furrer, D.F. McMorrow, K.W. Krämer, H.-U. Güdel, S.N. Gvasaliya, H. Mutka, and M. Boehm, Phys. Rev. Lett. **100**, 205701 (2008).
- ⁶⁴ P. Merchant, B. Normand, K.W. Krämer, M. Boehm, D.F. McMorrow, and Ch. Rüegg, Nat. Phys. **10**, 373 (2014).
- ⁶⁵ A. Malakis, A.N. Berker, I.A. Hadjiagapiou, and N.G. Fytas, Phys. Rev. E **79** 011125 (2009).
- ⁶⁶ A. Malakis, A.N. Berker, I.A. Hadjiagapiou, N.G. Fytas, and T. Papakonstantinou, Phys. Rev. E **81**, 041113 (2010).
- ⁶⁷ A. Malakis, A.N. Berker, N.G. Fytas, and T. Papakonstantinou, Phys. Rev. E **85**, 061106 (2012).
- ⁶⁸ E. Vatansever and N.G. Fytas, Phys. Rev. E **97**, 062146 (2018).
- ⁶⁹ A.W. Sandvik, Phys. Rev. Lett. **80**, 5196 (1998).
- ⁷⁰ M. Troyer, S. Wessel, and F. Alet, Phys. Rev. Lett. **90**, 120201 (2003).
- ⁷¹ A.W. Sandvik, AIP Conf. Proc. **1297**, 135 (2010).
- ⁷² A. Aharony and A.B. Harris, Phys. Rev. Lett. **77**, 3700 (1996).
- ⁷³ S. Wiseman and E. Domany, Phys. Rev. Lett. **81**, 22 (1998); Phys. Rev. E **58**, 2938 (1998).
- ⁷⁴ A.W. Sandvik, Phys. Rev. B **59**, R14157 (1999).
- ⁷⁵ A.W. Sandvik, J. Phys. A: Math. Gen. **25** 3667 (1992).
- ⁷⁶ Y.Q. Qin, B. Normand, A.W. Sandvik, and Z.Y. Meng, Phys. Rev. B **92**, 214401 (2015).
- ⁷⁷ A.W. Sandvik, Phys. Rev. B **56**, 11678 (1997).
- ⁷⁸ M. Wallin, E.S. Sørensen, S.M. Girvin, and A.P. Young, Phys. Rev. B **49**, 12115 (1994).
- ⁷⁹ L. Wang, K.S.D. Beach, and A.W. Sandvik, Phys. Rev. B **73**, 014431 (2006).
- ⁸⁰ M.E.J. Newman and G.T. Barkema, *Monte Carlo methods in Statistical Physics*, (Oxford University Press, New York, 1999).
- ⁸¹ J. Cardy, *Scaling and Renormalization in Statistical Physics*, (Cambridge University Press, 1996).
- ⁸² K. Binder, Z. Phys. B **43**, 119 (1981).
- ⁸³ T. Vojta, AIP Conf. Proc. **1550**, 188 (2013).